Draft version February 1, 2008
Preprint typeset using LaTeX style emulateapj v. 25/04/01



# MONTHLY 43 GHZ VLBA POLARIMETRIC MONITORING OF 3C 120 OVER 16 EPOCHS: EVIDENCE FOR TRAILING SHOCKS IN A RELATIVISTIC JET

José-Luis Gómez[1], Alan P. Marscher[2], Antonio Alberdi[1], Svetlana G. Jorstad[2] and Ivan Agudo[1]

*Draft version February 1, 2008*

## ABSTRACT

We present a 16-month sequence of monthly polarimetric 43 GHz VLBA images of the radio galaxy 3C 120. The images probe the inner regions of the radio jet of this relatively nearby superluminal radio galaxy at a linear resolution of 0.07 $h_{65}^{-1}$ pc ($H_o = 65\,h_{65}$ km s$^{-1}$ Mpc$^{-1}$). We follow the motion of a number of features with apparent velocities between 4.01±0.08 and 5.82±0.13 $h_{65}^{-1}$ $c$. A new superluminal knot, moving at $4.29 \pm 0.16$ $h_{65}^{-1}$ $c$, is observed to be ejected from the core at a time coincident with the largest flare ever observed for this source at millimeter wavelengths. Changes in the position angle of this component, as well as a progressive rotation of its magnetic polarization vector, suggest the presence of a twisted (resembling a helix in projection) configuration of the underlying jet magnetic field and jet geometry. We identify several knots that appear in the wake of the new superluminal component, moving at proper motions $\sim 4$ times slower than any of the other moving knots observed in 3C 120. These features have properties similar to those of the "trailing" shocks seen in relativistic, time-dependent, hydrodynamical and emission simulations of compact jets. Such trailing compressions are triggered by pinch-mode jet-body instabilities caused by the propagation of a strong perturbation, which we associate with the new strong superluminal component.

*Subject headings:* galaxies: active – galaxies: individual (3C 120) – galaxies: jets – polarization – radio continuum: galaxies

## 1. INTRODUCTION

The radio galaxy 3C 120 (redshift $z$=0.033) is a powerful and variable emitter of radiation at radio to X-ray frequencies, probably powered by a central black hole of at least $3 \times 10^7 M_\odot$ (Maraschi et al. 1991; Wandel, Peterson, & Malkan 1999). It was among the first radio jets in which apparent superluminal motion was detected (Seielstad et al. 1979; Walker, Benson, & Unwin 1987; Benson et al. 1988; Walker 1997). Previous observations using the Very Long Baseline Array (VLBA) at 22 and 43 GHz (Gómez et al. 1998) reveal a very rich inner jet structure containing up to ten different superluminal components. Coordinated Millimeter VLBI Array (CMVA) observations at 86 GHz (Gómez, Marscher, & Alberdi 1999), at an angular resolution of 54 $\mu$as, provide an upper limit to the size of the core of $\sim 1$ lt-month. Results from long-term milliarcsecond-scale monitoring at 1.7, 5, and 10.7 GHz (Walker et al. 2001) allowed determination of superluminal motions up to at least 150 pc in projection from the core, as well as evidence for stationary features suggestive of a helical pattern viewed in projection.

Further monitoring at a higher frequency, consisting of 16 monthly polarimetric 22 GHz VLBA observations of 3C 120 (Gómez et al. 2000), explored a more compact region in the jet, where superluminal components undergo variations in total and linearly polarized flux densities on timescales of months. [A movie generated from these 16 total and polarized intensity images can be downloaded at *Science* Online (www.sciencemag.org/feature/data/1052657.shl).] In this *Letter*, we present 43 GHz images corresponding to the same epochs as the 22 GHz observations presented in Gómez et al. (2000).

## 2. OBSERVATIONS AND DATA ANALYSIS

We observed 3C 120 with the 10 antennas of the VLBA at a frequency of 43 GHz at the following epochs: 1997 Nov. 10, 1997 Dec. 11, 1998 Jan. 11, 1998 Feb. 7, 1998 Mar. 9, 1998 Apr. 10, 1998 May 9, 1998 June 11, 1998 July 11, 1998 Aug. 13, 1998 Sept. 16, 1998 Oct. 26, 1998 Dec. 3, 1999 Jan 10, 1999 Feb. 10, and 1999 Mar. 19. The data were recorded in 1-bit sampling VLBA format with 32 MHz bandwidth per circular polarization. Reduction of the data was performed with the AIPS software in the usual manner (e.g., Leppänen, Zensus, & Diamond 1995). Opacity corrections were introduced by solving for receiver temperature and zenith opacity at each antenna. The instrumental polarization was determined using the feed-solution algorithm developed by Leppänen, Zensus, & Diamond (1995). The feed D-terms (instrumental polarization) were found to be very consistent over all sources observed and to remain stable. The absolute phase offset between right- and left-circularly polarized data (which determines the polarization position-angle calibration) was obtained by comparison of the integrated polarization of the VLBA images of several compact sources (0420-014, OJ287, BL Lac, and 3C 454.3) with 14 Very Large Array (VLA) observations at epochs 1997 Nov. 21, 1999 Dec. 14, 1998 Jan. 15, 1998 Feb. 12, 1998 Mar. 7, 1998 Apr. 8, 1998 June 9, 1998 July 11, 1998 Aug. 14, 1998 Sep. 19, 1998 Oct. 29, 1998 Nov. 28, 1999 Feb. 17, and 1999

[1] Instituto de Astrofísica de Andalucía, CSIC, Apartado 3004, 18080 Granada, Spain. jlgomez@iaa.es; antxon@iaa.es; ivan@iaa.es
[2] Institute for Astrophysical Research, Boston University, 725 Commonwealth Avenue, Boston, MA 02215, USA. marscher@bu.edu; jorstad@rjet.bu.edu

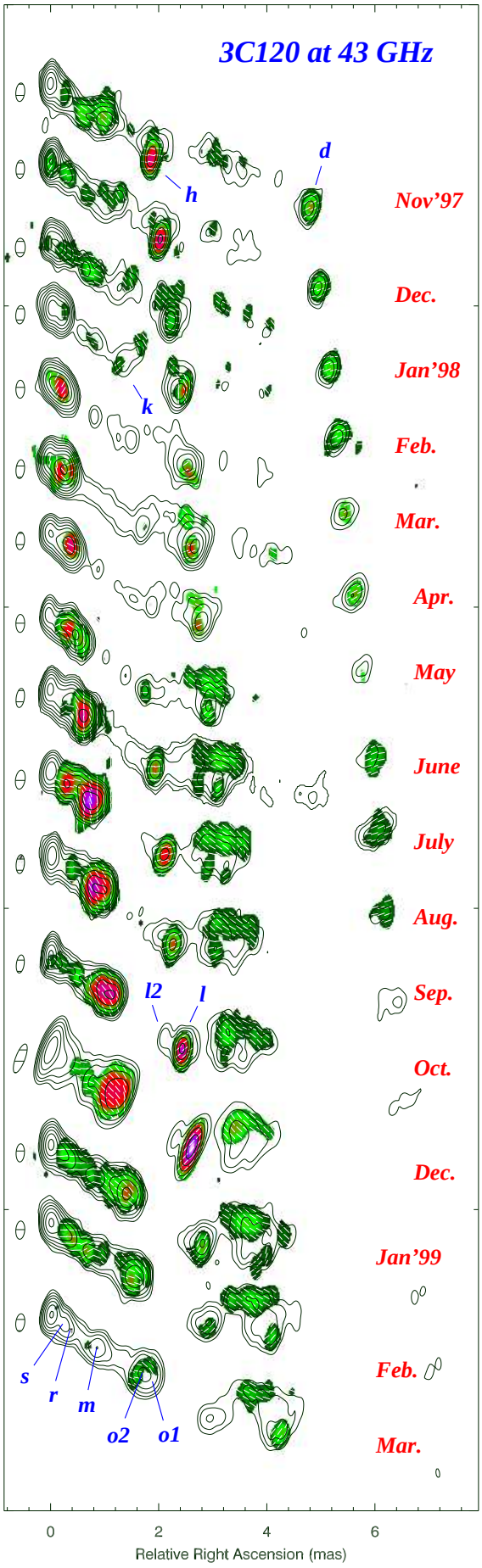


FIG. 1.— VLBA images of 3C 120 at 43 GHz. Epochs of observation are indicated to the right of each image. Vertical image separation is proportional to the time difference between epochs of observation. Contours give the total intensity, colors (on a linear scale from green to white) show the polarized intensity, and bars (of unit length) indicate the direction of the magnetic polarization vector. Synthesized beams are plotted to the left of each image, with a typical size of 0.35×0.16 mas. The peak brightness (r.m.s. noise) in polarization corresponds to 32.4 mJy beam$^{-1}$ (1.4 mJy beam$^{-1}$). Contour levels for all epochs are in factors of 2 of the bottom level of 4.4 mJy/beam, except for epochs Feb'98, May'98, Jul'98, Aug'98, Oct'98, Dec'98, and Jan'99 for which the bottom contour level is 8.8 mJy/beam. For epoch Jun'98 an extra contour at 2.2 mJy/beam has been plotted. No data was obtained in MK station for epoch Dec'98, which resulted in a larger synthesized beam.

Mar. 17. Estimated errors in the orientation of the polarization vectors vary from epoch to epoch, but usually lie in the range of 7–15°, confirmed by the stability of the D-terms across epochs (Gómez et al., in preparation).

## 3. RESULTS

The images, plotted in Fig. 1, reveal a rich, variable structure in both total and linearly polarized intensity. In order to identify and follow discrete features across epochs, we performed model fits of the $u$-$v$ data with circular Gaussian components using the software Difmap (Shepherd 1997), which was also used to edit the data and make the final images. Figure 2 shows the positions and magnetic polarization direction for the fitted components at all epochs. Inspection of this figure reveals that, at a distance of approximately 2 mas from the core (the closest distance at which we can resolve the jet across its width), bright features usually lie near the edge of the jet, suggesting limb brightening. This stratification is even more apparent in polarization: Magnetic vectors on the northern side of the jet are oblique to the jet axis but constant in orientation, while those on the southern side rotate as the polarized emission features move downstream (e.g., components $h$ and $l$ in Fig. 2). This is similar to the behavior observed at 22 GHz (Gómez et al. 2000).

### 3.1. *Superluminal Components*

Because of the complexity and temporal variability of the jet, some of the fitted components cannot easily be identified across epochs. We concentrate our discussion on those features that can be followed reliably. Six of these components, those labeled in Fig. 1 as $o$ (containing components *o1* and *o2*), *l2*, *l*, *k*, *h*, and *d*, separate from the core at apparent superluminal velocities (proper motions) of 4.29±0.16 (1.83±0.07), 5.38±0.08 (2.29±0.04), 5.10±0.14 (2.17±0.06), 5.82±0.13 (2.48±0.05), 4.12±0.06 (1.75±0.03), and 4.01±0.08 $h_{65}^{-1}$ c (1.71±0.03 mas yr$^{-1}$), respectively. The separation of these components from the core versus time is plotted in Fig. 3.

As observed at 22 GHz (Gómez et al. 2000), components $h$ and $l$ brighten markedly when reaching a distance of about 3 mas from the core (see Figs. 1 and 2). Gómez et al. explained this brightening, accompanied by a rotation of the magnetic polarization vector, as interaction between the jet and a cloud with properties intermediate between those of the broad and narrow emission-line regions.

The inner jet structure in Fig. 1 is dominated by the

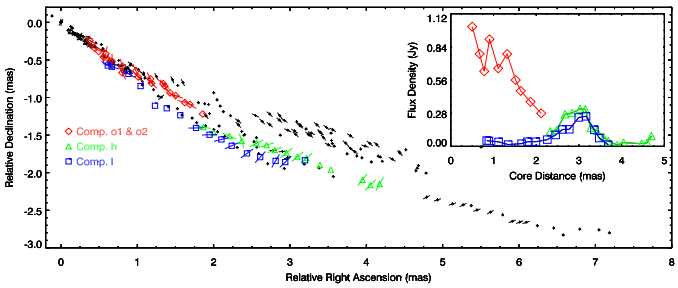


FIG. 2.— Positions and magnetic polarization vector orientations of the components obtained from model fitting of the images shown in Fig. 1. Components *o1*, *o2*, *h*, and *l* have been highlighted with different symbols and colors, with their light curves plotted in the inset panel. The integrated flux density is plotted at the position of the brightness centroid for components *o1* and *o2*.

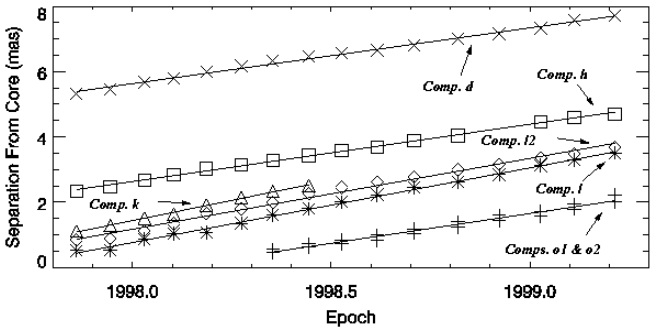


FIG. 3.— Projected angular distance from the core as a function of time for the superluminal components found in 3C 120. Lines show a minimum $\chi^2$ linear fit for each component. A common fit has been used for components *o1* and *o2*.

appearance of a new component near the beginning of the largest mm-wave flare ever observed in 3C 120 (H. Teräsranta, private communication). By epoch 1997 December 14 the core had brightened significantly (see Fig. 4), after which the new component (*o*), appeared downstream of the core (Fig. 1). Figure 4 shows that component *o* presents an extended emission structure that can be split into three different features (those marked in red in Fig. 4) between 1998 January 11 and 1998 April 10. These probably do not represent distinct entities, but rather correspond to complexity in the internal brightness distribution, reminiscent of the pattern of major disturbances in numerical simulations (Gómez et al. 1997). By epoch 1998 May 9 the front of knot *o* is futher resolved into two subcomponents, labeled *o1* and *o2*, with proper motions of 1.87±0.05 mas yr$^{-1}$ (4.40±0.12 $h_{65}^{-1}$ c) and 1.78±0.05 mas yr$^{-1}$ (4.19±0.11 $h_{65}^{-1}$ c), respectively. The epoch of ejection (i.e., extrapolated date of coincidence with the core) of component *o1* is 1998.07±0.03 (see Fig. 4).

Although components *o1* and *o2* move with a relatively constant proper motion, Fig. 5a (see also Fig. 2) shows that the lines between their positions and that of the core vary by 7° as they move between ∼0.5 and 2.0 mas from the core. Furthermore, these variations in position angle are accompanied by rotation of the magnetic polarization vectors with respect to the local jet axis, as shown in Fig. 5b (see also Fig. 2). The initially perpendicular magnetic vector at epoch 1998 March 9 is observed to align with the jet axis by 1998 May 8. This is followed by a rotation of about 60° by 1998 June 11. The magnetic vector subsequently rotates more slowly in components *o1* and *o2* until it becomes approximately aligned to the jet axis during the final epochs. Opacity effects, which can produce a rotation of 90° (as observed in OJ 287; Gabuzda & Gómez 2001), could only be present at epoch 1998 March 9, when component *o* has a nearly flat spectrum ($\alpha \sim -0.06$, $S_\nu \propto \nu^\alpha$); at the other epochs components *o1* and *o2* have steep, optically thin spectra.

Although Faraday rotation could contribute to the observed rotation of the magnetic polarization vectors, an alternative interpretation would be the existence of an underlying helical magnetic field with a progressively increasing pitch angle until the magnetic field becomes aligned (as observed at larger scales, Walker, Benson, & Unwin 1987). This would be in agreement with the observed variation in the position angles of the core-component separations and the twisted internal structure of component *o*, the latter of which is most clearly visible at epochs 1998 June 11, July 11, and August 13 (see Fig. 1). This interpretation would also agree with the suggested helical pattern at larger scales (Walker et al. 2001).

### 3.2. *Trailing Components*

By epoch 1998 May 9 we can distinguish two emission regions in the newly ejected component *o*: the front section (subcomponents *o1* and *o2*, plotted in green in Fig. 4) and the back section (*p*, plotted in blue in Fig. 4). The subsequent evolution of these two emission regions is significantly different: While *o1* and *o2* move with a relatively constant proper motion, Fig. 4 shows that *p* splits into two parts that progressively decelerate and decrease in total flux more rapidly than do *o1* and *o2*. Acceleration is also observed to take place later in component *m2*. By epoch 1998 September 16 a similar split takes place, leading to the appearance of components *m* and *m1*. The evolution of the jet following the disturbance that created component *o* therefore involves steady, fast superluminal motion at the front, followed by the (in some cases temporary) appearance of slower secondary features in the wake.

The last epochs in Figs. 1 and 4 show that the strongest feature in the wake of component *o* is that labeled *m*. This component, which maintains a relatively constant flux density of ∼100 mJy, moves at an apparent speed of 1.16±0.22 $h_{65}^{-1}$c (0.49±0.09 mas yr$^{-1}$). This is a factor ∼ 4 slower than any of the other moving components detected in 3C 120 (see Fig. 3). Images at 22 GHz (Gómez et al. 2000) also contain component *m*, but with a proper motion compatible with stationarity (−0.35±1.10 mas yr$^{-1}$); however, the resolution was about twice as coarse as that at 43 GHz. The polarization of *m* is strong at 22 GHz, with magnetic vector direction (relative to the direction between *m* and the core) of 24, 19, and 27° and degree of polarization of 25, 20, and 15%, at epochs 1999 January 10, 1999 February 10 and 1999 March 19, respectively. Two components even closer to the core, labeled *r* and *s*, are also apparent in Fig. 4. Their proper motions are the slowest detected in 3C 120: 0.40±0.03 mas yr$^{-1}$ (0.93±0.07 $h_{65}^{-1}$ c) and 0.27±0.07 mas yr$^{-1}$ (0.63±0.17 $h_{65}^{-1}$ c) for *r* and *s*, respectively.

The nature of the components that appear on the wake of component *o* is consistent with the characteristics of the trailing

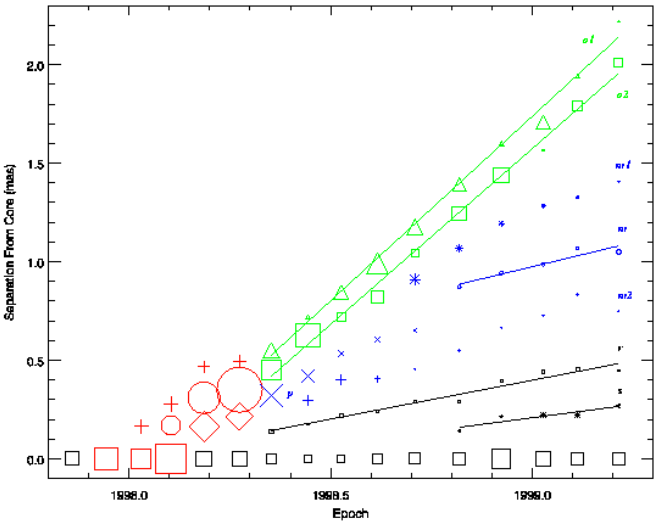


FIG. 4.— Projected angular distance from the core vs. time for the jet features between component *o1* and the core. The symbol size is proportional to the component's total flux density. Those features associated with the initial evolution of component *o* are plotted in red. By epoch 1998 May 9 this component can be resolved into two different sets of subcomponents, each with a different development: those marked in green (for components *o1* and *o2*), and those in blue, corresponding to the trailing components.

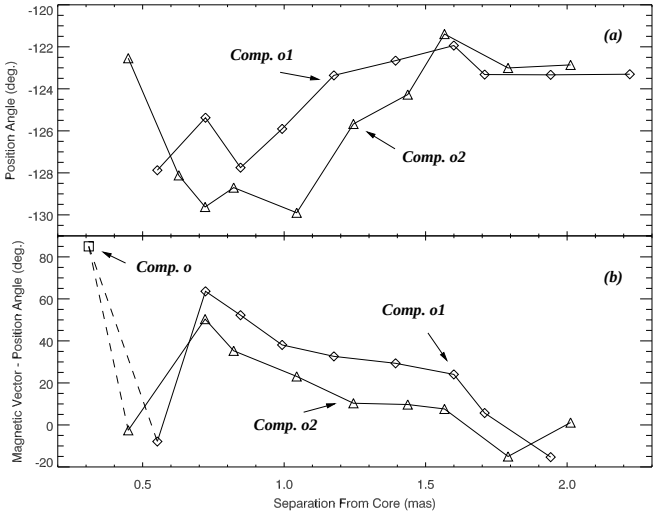


FIG. 5.— *(a, top)* Position angle and *(b, bottom)* orientation of the magnetic polarization vector relative to the core position angle for components *o*, *o1*, and *o2* as a function of projected angular distance from the core.

features that appear behind a major flow disturbance in relativistic time-dependent hydrodynamical and emission simulations of jets (Agudo et al. 2001). These simulations show that strong jet perturbations (which we associate with bright superluminal knots) interact with the underlying jet and external medium as they propagate. This leads to the formation of recollimation shocks and rarefactions in the wake of the main perturbation. These formations are triggered by pinch body jet instabilities. Agudo et al. (2001) predict that trailing components should appear to split from the primary component rather than emerge from the core, and to have significantly slower proper motions than that of the leading strong knot. The apparent velocities of the trailing features should range from subluminal closest to the core to more superluminal near the leading knot. This is in good agreement with the nature of component *m*, which indeed appears to split from component *o* and to move at a slower speed. Alternatively, component *m* may correspond to a reverse shock of component *o* that is slower than the forward shock represented by subcomponents *o1* and *o2* in this interpretation. The subluminal motions of components *r* and *s* are also consistent with the predictions for trailing components.

The good agreement between the changing emission pattern observed in 3C 120 and the structures predicted by 2-D, relativistic, cylindrically symmetric hydrodynamical and emission simulations (Agudo et al. 2001) points to the value of such computations for interpreting observations of real jets. Three-dimensional simulations that are now becoming available promise to provide even more realistic comparisons.

This research was supported in part by Spain's Dirección General de investigación Científica y Técnica (DGICYT) grant PB97-1164, by US National Science Foundation (NSF) grant AST-9802941, and by Fulbright commission for collaboration between Spain and the United States. The VLBA and VLA are instruments of the National Radio Astronomy Observatory, a facility of the NSF operated under cooperative agreement by Associated Universities Inc. We are grateful to Barry Clark for scheduling *ad hoc* VLA time in order to determine the polarization position angle calibration.

## REFERENCES

Agudo, I., Gómez, J. L., Martí, J. M., Ibáñez, J. M., Marscher, A. P., Alberdi, A., Aloy, M. A., Hardee, P. E. 2001, ApJ, 549, L183
Benson, J. M., Walker, R. C., Unwin, S. C., Muxlow, T. W. B., Wilkinson, P. N., Booth, R. S., Pilbratt, G., & Simon, R. S. 1988, ApJ, 334, 560
Gabuzda, D. C., & Gómez, J. L. 2001, MNRAS, 320, L49
Gómez, J. L., Martí, J. M., Marscher, A. P., Ibáñez, J. M., & Alberdi, A. 1997, ApJ, 482, L33
Gómez, J. L., Marscher, A. P., Alberdi, A., Martí, J. M., & Ibáñez, J. M. 1998, ApJ, 499, 221
Gómez, J. L., Marscher, A. P., Alberdi, A. 1999, ApJ, 521, L29
Gómez, J. L., Marscher, A. P., Alberdi, A., Jorstad, S. G., García-Miró, C. 2000, Science, 289, 2317
Leppänen, K. J., Zensus, J. A., & Diamond, P. J. 1995, AJ, 110, 2479
Maraschi, L., Chiapetti, L., Falomo, R., Garilli, B., Malkan, M., Tagliaferri, G., Tanzi, E. G., & Treves, A. 1991, ApJ, 368, 138
Seielstad, G. A., Cohen, M. H., Linfield, R. P., Moffet, A. T., Romney, J. D., Schilizzi, R. T., & Shaffer, D. B. 1979, ApJ, 229, 53
Shepherd, M. C. 1997, in Astronomical Data Analysis Software and Systems VI, Astron. Soc. Pac. Conf. Proc., 125
Walker, R. C., Benson, J. M., & Unwin, S. C. 1987, ApJ, 316, 546
Walker, R. C. 1997, Apj, 488, 675
Walker, R. C., Benson, J. M., Unwin, S. C., Lystrup, M. B., Hunter, T. R., Pilbratt, G., & Hardee, P. E. 2001, ApJ, in press (available as astro-ph/0103379)
Wandel, A., Peterson, B. M., & Malkan, M. A. 1999, ApJ, 526, 579